EurJIC European Journal of Inorganic Chemistry
ChemPubSoc Europe
FULL PAPER

DOI:10.1002/ejic.201402236

Cycloruthenation of *N*-(Naphthyl)salicylaldimine and Related Ligands: Utilization of the Ru–C Bond in Catalytic Transfer Hydrogenation

Jayita Dutta,[a] Michael G. Richmond,[b] and Samaresh Bhattacharya*[a]

Dedicated to Professor Cortlandt G. Pierpont[‡]

Keywords: Homogeneous catalysis / C–H activation / Hydrogenation / Ruthenium

Upon reaction with $[Ru(PPh_3)_2(CO)_2Cl_2]$, *N*-(naphthyl)-4-R-salicylaldimines (R = OCH_3, H, Cl; $H_2\mathbf{L^1}$–$H_2\mathbf{L^3}$) and 2-hydroxy-*N*-(naphthyl)naphthaldimine ($H_2\mathbf{L^4}$) readily undergo cycloruthenation by C–H bond activation at the *peri* position to afford complexes of the type $[Ru(PPh_3)_2(\mathbf{L})(CO)]$ ($\mathbf{L} = \mathbf{L^1}$–$\mathbf{L^4}$). The crystal structures of the $[Ru(PPh_3)_2(\mathbf{L})(CO)]$ ($\mathbf{L} = \mathbf{L^1}$, $\mathbf{L^2}$, $\mathbf{L^4}$) complexes were determined and the structure of $[Ru(PPh_3)_2(\mathbf{L^3})(CO)]$ optimized by DFT calculations. The thermodynamics for the reaction of $[Ru(PPh_3)_2(CO)_2Cl_2]$ with $H_2\mathbf{L^2}$ to give $[Ru(PPh_3)_2(\mathbf{L^2})(CO)]$ were determined. All the complexes show intense absorptions in the visible and UV regions, which have been analyzed by TDDFT calculations. Cyclic voltammetry of the four cycloruthenated complexes showed two oxidations within the range 0.50–1.35 V versus SCE and a reduction at around –1.75 V versus SCE. The $[Ru(PPh_3)_2(\mathbf{L})(CO)]$ ($\mathbf{L} = \mathbf{L^1}$–$\mathbf{L^4}$) complexes were found to efficiently catalyze the transfer hydrogenation of carbonyl compounds.

Introduction

The chemistry of ruthenium complexes continues to receive considerable attention from a diverse group of researchers, primarily because of their fascinating redox, photophysical, and photochemical properties.[1] Another property of the ruthenium complexes that has gained prominence over the years is their efficiency in catalyzing a wide variety of industrially important reactions.[2] Particularly notable is the increasing tendency of utilizing ruthenium complexes as catalysts to effect useful organic transformations.[3] The majority of these transformations are known to involve the participation of a reactive organo-ruthenium intermediate, which is generated in situ usually by activation of a C–H bond. Ensuing reactions with the resulting Ru–C fragment afford the desired end-product(s). Studies of Ru–C bonded species, with particular reference to their formation and reactivity, serve to increase our knowledge base of such fundamental catalytic intermediates and are therefore of significant contemporary importance; the impetus for the present work derives from our interest in these two aspects of ruthenium chemistry. A group of four Schiff bases,

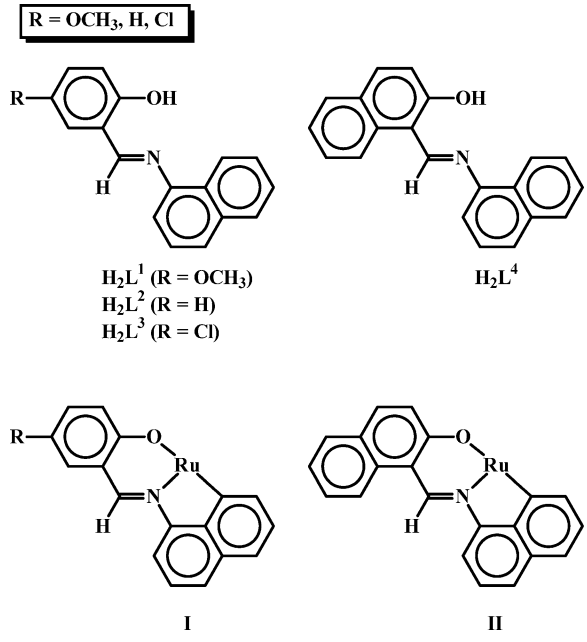

Figure 1. Aldimine ligands $H_2\mathbf{L^1}$–$H_2\mathbf{L^4}$ and their expected mode of coordination (**I** and **II**) with ruthenium.

[a] Department of Chemistry, Inorganic Chemistry Section, Jadavpur University, Kolkata 700032, India
http://www.jaduniv.edu.in
[b] Department of Chemistry, University of North Texas, Denton, TX 76203, USA
[‡] University of Colorado at Boulder, USA
Supporting information for this article is available on the WWW under http://dx.doi.org/10.1002/ejic.201402236.

namely three *N*-(naphthyl)salicylaldimines (H_2L^1–H_2L^3) and 2-hydroxy-*N*-(naphthyl)naphthaldimine (H_2L^4), were chosen as the principal ligands for the present study (Figure 1). The initial goal was to induce an ONC mode of coordination (**I** and **II**; Figure 1) by these ligands, which requires the loss of two protons from the uncoordinated ligand, the phenolic proton and the naphthyl proton at the *peri* position, and hence the selected ligands are abbreviated in general as H_2L, in which H_2 represents the two protons that are released upon ligand coordination. It is relevant to mention that although salicylaldimines and related ligands have been exhaustively studied as ligand auxiliaries with many transition-metal ions,[4] the ruthenium complexes of such ligands have received less attention.[5] The ability of the selected aldimine ligands (H_2L^1–H_2L^4) to furnish cycloruthenated complexes containing chelate **I** or **II** is best investigated by using $[Ru(PPh_3)_2(CO)_2Cl_2]$ as the starting ruthenium complex due to its demonstrated ability to accommodate dianionic tridentate chelating ligands through the displacement of carbonyl and chlorides.[6] Herein we report on the reactions of the selected aldimine ligands H_2L^1–H_2L^4 with $[Ru(PPh_3)_2(CO)_2Cl_2]$, which have indeed afforded cycloruthenated complexes. The new complexes were fully characterized by a combination of spectroscopic methods, X-ray diffraction analysis, and DFT calculations, and their ability to serve as precursors in the catalytic transfer hydrogenation of a wide variety of aldehydes and ketones is discussed.

Results and Discussion

Formation and Structure

As outlined in the introduction, the primary goal of this study was to explore the possibility of obtaining cycloruthenated species by activation of the C–H bond at the *peri* position of the *N*-naphthyl ring in the four selected aldimine ligands (H_2L^1–H_2L^4) through their interaction with $[Ru(PPh_3)_2(CO)_2Cl_2]$. The planned reactions proceeded smoothly in 2-methoxyethanol at reflux in the presence of triethylamine, and from each of these reactions an orange complex was obtained in good yield. Preliminary characterization (microanalysis, NMR, and IR) of these complexes indicated the presence of a doubly deprotonated aldimine ligand, two triphenylphosphines, and a carbonyl in the ruthenium coordination sphere. Hence these complexes were formulated in general as $[Ru(PPh_3)_2(L)(CO)]$ (**L** = L^1–L^4). For an unambiguous characterization of these complexes, with particular reference to the coordination mode exhibited by the aldimine ligand, the solid-state structure of $[Ru(PPh_3)_2(L^1)(CO)]$ was determined by X-ray crystallography. The structure is shown in Figure 2 and selected bond parameters are presented in Table 1. The structure confirms that the *N*-(naphthyl)salicylaldimine is coordinated to the ruthenium center in the targeted ONC fashion (**I**, R = OCH_3), forming two adjacent six- and five-membered chelate rings with bite angles of 87.54(14) and 80.64(17)°, respectively. Two triphenylphosphines and a carbonyl are also coordinated to the metal center. The meridionally disposed ONC ligand and the carbonyl group define the equatorial plane with ruthenium at the center of this six-coordinate complex; the two PPh_3 ligands occupy the remaining two axial positions and are situated in a mutually *trans* orientation. Ruthenium is thus nested in a C_2NOP_2 coordination environment, which is distorted significantly from an ideal octahedral geometry, as reflected in the metric param-

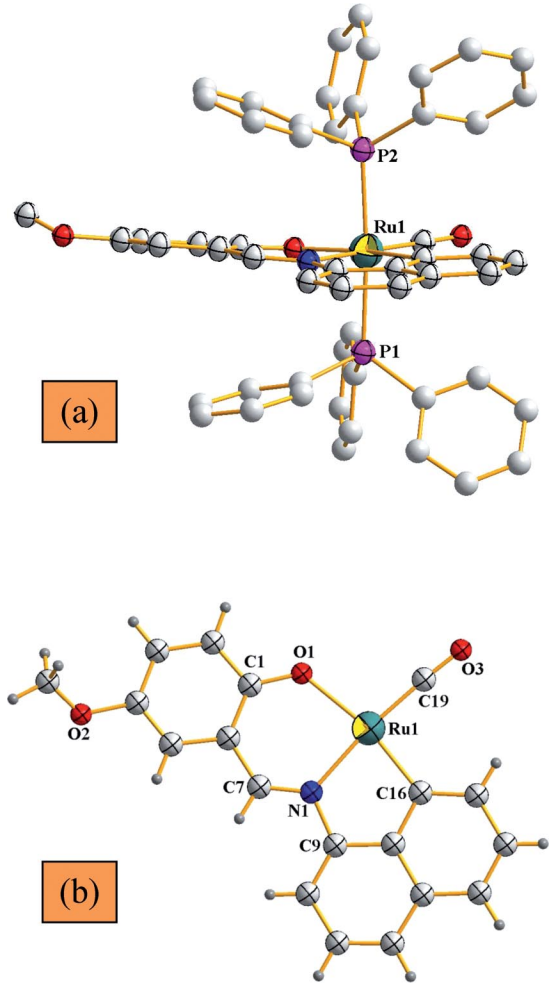

Figure 2. (a) Crystal structure of $[Ru(PPh_3)_2(L^1)(CO)]$ (hydrogen atoms have been omitted for clarity) and (b) view of the equatorial plane.

Table 1. Selected bond lengths and bond angles for $[Ru(PPh_3)_2(L^1)(CO)]$.

Bond lengths [Å]			
Ru1–O1	2.136(3)	C1–O1	1.308(7)
Ru1–N1	2.111(4)	C7–N1	1.298(6)
Ru1–C16	2.038(4)	C9–N1	1.432(5)
Ru1–C19	1.815(6)	C19–O3	1.169(7)
Ru1–P1	2.387(1)		
Ru1–P2	2.382(1)		
Bond angles [°]			
N1–Ru1–C19	173.2(2)	O1–Ru1–N1	87.5(1)
O1–Ru1–C16	168.0(2)	N1–Ru1–C16	80.6(2)
P1–Ru1–P2	175.22(4)	Ru1–C19–O3	176.7(4)

eters around the metal center (Table 1). The Ru–C, Ru–N, Ru–O, and Ru–P bond lengths are in accord with the corresponding distances in related compounds published by us.[6] The existence of noncovalent interactions between individual molecules of the complex is reinforced by the absence of any solvent of crystallization in the lattice, and this is illustrated by the packing diagram depicted in Figure 3. The important intermolecular hydrogen-bonding interactions extant in the unit cell consist of five types, namely (azomethine)C–H···O(carbonyl), (naphthyl)C–H···O(carbonyl), (PPh_3 phenyl)C–H···O(methoxy), (methoxy)C–H···π(phenyl of PPh_3), and (PPh_3 phenyl)C–H···π(phenyl of PPh_3), and involve different fragments of coordinated ligands. The metric parameters associated with these hydrogen-bonding interactions are presented in Table 2. Each complex molecule is thus linked to five surrounding complex molecules through the above interactions, which extend throughout the lattice and are responsible for the stability of the crystal.

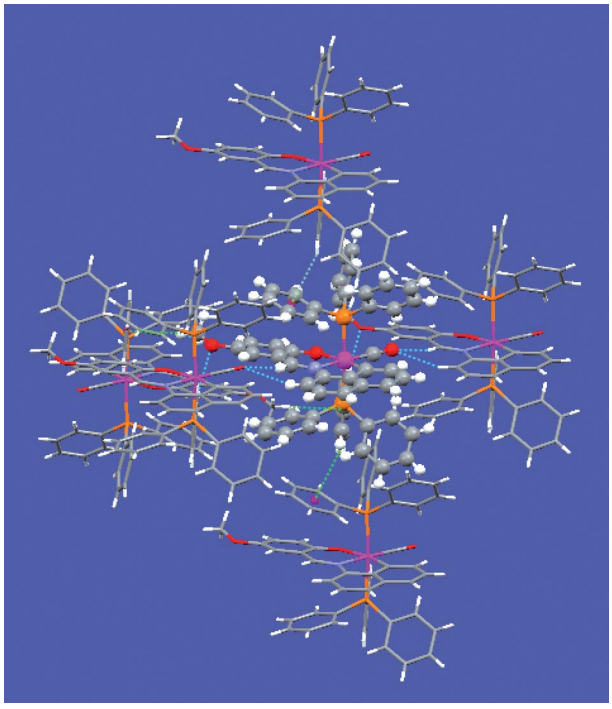

Figure 3. Intermolecular C–H···O and C–H···π interactions in the lattice of $[Ru(PPh_3)_2(\mathbf{L^1})(CO)]$.

The structural characterization of $[Ru(PPh_3)_2(\mathbf{L^1})(CO)]$ confirmed the binding of the $H_2\mathbf{L^1}$ ligand in the expected ONC mode (**I**, R = OCH_3), which is facilitated by the activation of the C–H bond at the *peri* position of the naphthyl ring. To ascertain the generality of the ONC coordination mode in the other three $[Ru(PPh_3)_2(\mathbf{L})(CO)]$ complexes (**L** = $\mathbf{L^2}$, $\mathbf{L^3}$, $\mathbf{L^4}$), attempts were made to determine the molecular structure of the other compounds. We determined the structures of $[Ru(PPh_3)_2(\mathbf{L^2})(CO)]$ and $[Ru(PPh_3)_2(\mathbf{L^4})(CO)]$ by X-ray crystallography (Figure 4, Figure 5, and Table S1 in the Supporting Information), and found that the aldimine ligand in both structures binds the ruthenium center in the same ONC mode (**I**, R = Cl, and **II**). Although a structure determination of $[Ru(PPh_3)_2(\mathbf{L^3})(CO)]$ was precluded by our inability to grow suitable crystals for X-ray diffraction analysis, we analyzed $[Ru(PPh_3)_2(\mathbf{L^3})(CO)]$ computationally by density functional theory (DFT) using the B3LYP functional;[7] the geometry optimization was performed on the PMe_3 derivative to reduce the total number of atoms and simplify the calculation. The DFT-optimized

Table 2. C–H···O and C–H···π interactions in the crystal lattice of $[Ru(PPh_3)_2(\mathbf{L^1})(CO)]$.

C–H···O interactions C–H···O	C–H [Å]	H···O [Å]	C···O [Å]	C–H···O [°]
(azomethine)C–H···O(carbonyl)	0.929	2.567	3.472	164.60
(naphthyl)C–H···O(carbonyl)	0.920	2.660	3.553	159.65
(PPh_3 phenyl)C–H···O(methoxy)	0.931	2.596	3.459	154.46
C–H···π interactions[a] **C–H···π**	**C–H [Å]**	**H···R [Å]**	**C···R [Å]**	**C–H···R [°]**
(methoxy)C–H···π(phenyl of PPh_3)	0.959	3.110	3.836	133.70
(PPh_3 phenyl)C–H···π(phenyl of PPh_3)	0.930	3.007	3.820	146.78

[a] R denotes the centroid of the phenyl ring.

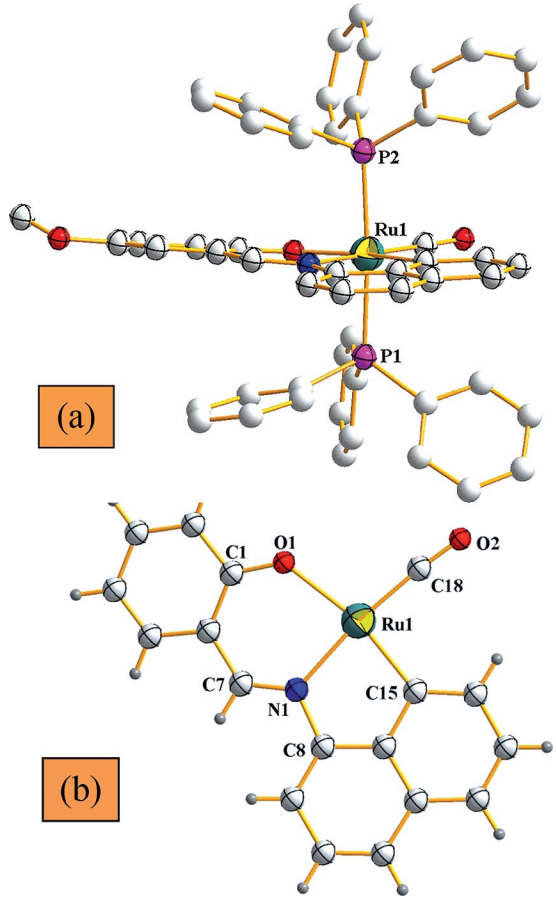

Figure 4. (a) Crystal structure of $[Ru(PPh_3)_2(\mathbf{L^2})(CO)]$ (hydrogen atoms have been omitted for clarity) and (b) view of the equatorial plane.

structure for $[Ru(PMe_3)_2(\mathbf{L^3})(CO)]$ is shown in Figure 6, and a selection of the computed bond parameters are listed in Table S2 in the Supporting Information. The DFT-optimized structure of $[Ru(PMe_3)_2(\mathbf{L^3})(CO)]$ is in good agreement with the experimentally determined crystal structures of the other three $[Ru(PPh_3)_2(\mathbf{L})(CO)]$ ($\mathbf{L} = \mathbf{L^1}$, $\mathbf{L^2}$, $\mathbf{L^4}$) complexes.

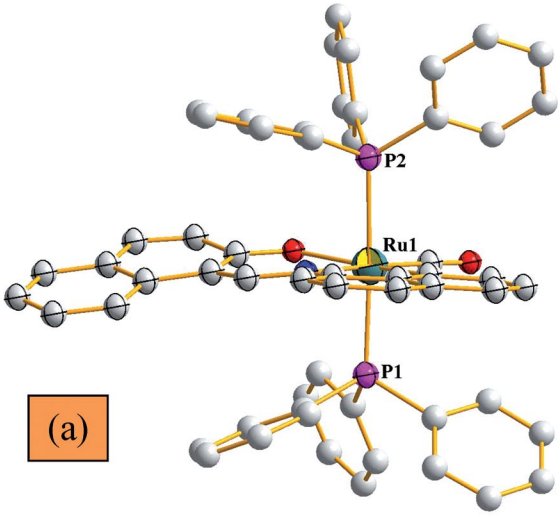

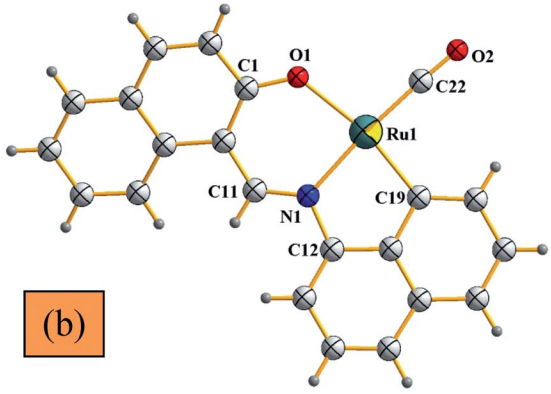

Figure 5. (a) Crystal structure of $[Ru(PPh_3)_2(\mathbf{L^4})(CO)]$ (hydrogen atoms have been omitted for clarity), and (b) view of the equatorial plane.

The formation of the cycloruthenated $[Ru(PPh_3)_2(\mathbf{L})(CO)]$ complexes is believed to involve several steps, which are illustrated in Scheme 1 for the reaction between $[Ru(PPh_3)_2(CO)_2Cl_2]$ and $H_2\mathbf{L^2}$. In the initial step, the aldimine ligand is assumed to react with $[Ru(PPh_3)_2(CO)_2Cl_2]$ and bind to the metal center by dissociation of the phenolic proton, as a monoanionic ON donor, coupled with simultaneous dissociation of a carbonyl and chloride from the ruthenium starting complex to generate intermediate **A**. Under the prevailing experimental conditions, **A** is believed to isomerize to **B** by mutual exchange of the positions of the carbonyl and chloride ligands. In **B** the naphthyl proton at the *peri* position is in close proximity to the ruthenium-

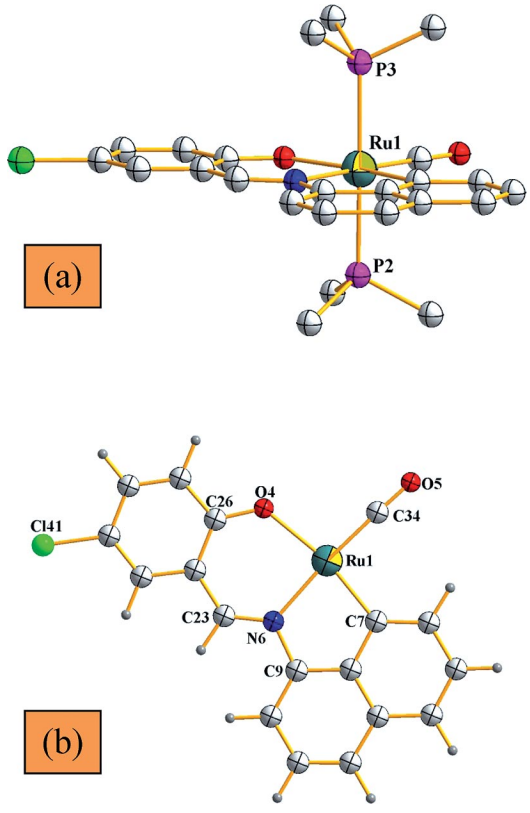

Figure 6. (a) DFT-optimized structure of $[Ru(PMe_3)_2(\mathbf{L^3})(CO)]$ (hydrogen atoms have been omitted for clarity) and (b) view of the equatorial plane.

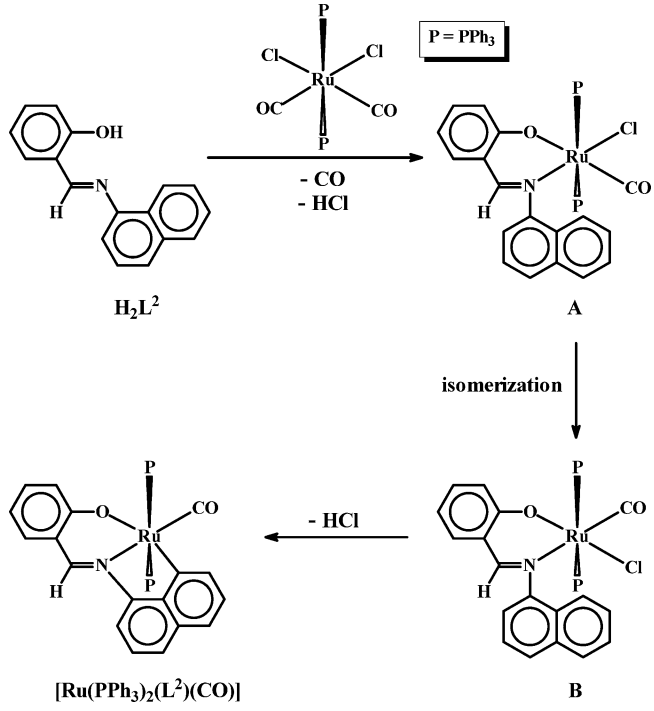

Scheme 1. Probable steps leading to the formation of the $[Ru(PPh_3)_2(\mathbf{L})(CO)]$ complexes.

bound chloride, which triggers the elimination of HCl leading to the formation of the $[Ru(PPh_3)_2(\mathbf{L^2})(CO)]$ complex.

The starting ruthenium complex, $[Ru(PPh_3)_2(CO)_2Cl_2]$, and the Schiff base H_2L^2 were optimized by DFT, as were the remaining species depicted in Scheme 1. Stable geometries, with only positive eigenvalues, were found for each species, and this allowed us to determine the thermodynamics for the observed transformation that affords $[Ru(PPh_3)_2(L^2)(CO)]$. Equation (1) shows the stoichiometrically balanced reaction, the net free energy (ΔG) of which was computed to be 32.7 kcal mol^{-1}. The enthalpy change was computed to be 49.5 kcal mol^{-1}, and this confirms the fact that the reaction is entropically driven (ΔS = 56 e.u.) through the release of CO and HCl byproducts.

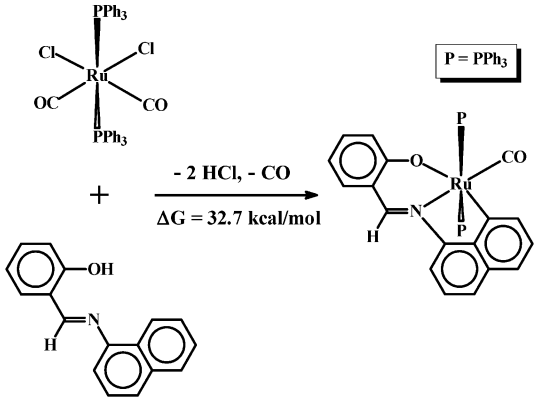

(1)

Spectral Properties

The IR spectra of the $[Ru(PPh_3)_2(L)(CO)]$ (L = L^1–L^4) complexes show many bands of varying intensities within the range 4000–450 cm^{-1}, but assignment of each individual band to a specific vibration has not been attempted. However, the strong band displayed at around 1900 cm^{-1} by all the complexes has been attributed to the coordinated carbonyl, and the three strong bands at around 518, 694, and 742 cm^{-1} indicate the presence of coordinated PPh_3 ligands. In the coordinated aldimine ligands, the C=N stretch has been identified in all the complexes as a strong band in the range 1592–1615 cm^{-1}, and a sharp band at around 1093 cm^{-1} has been assigned to the phenolic C–O stretch.

Magnetic susceptibility measurements revealed that the $[Ru(PPh_3)_2(L)(CO)]$ (L = L^1–L^4) complexes are diamagnetic, which corresponds to the presence of a bivalent ruthenium (low-spin d^6, S = 0). The NMR spectra of these complexes were recorded in $CDCl_3$ solution, and the NMR data are presented in the Exp. Sect. In the ^{1}H NMR spectra, broad signals are observed at 6.96–7.24 ppm, which correspond to the triphenylphosphines. Most of the expected signals from the ONC-coordinated aldimine ligands are clearly observed, but a few individual resonances could not be identified due to extensive overlap. For example, the azomethine proton signal is observed as a distinct peak within the range 7.27–8.35 ppm, and in $[Ru(PPh_3)_2(L^1)(CO)]$ the signal for the OCH_3 group was observed at δ = 3.57 ppm. The ^{13}C NMR spectra of these complexes show all the expected signals. The most deshielded signal at around 208 ppm has been attributed to the carbonyl carbon, and the next deshielded signal, observed at around 170 ppm, to the ruthenium-bound *peri* carbon of the naphthyl ring. The ^{31}P NMR spectra of all the complexes show a single resonance within the range 32.53–34.71 ppm, which indicates the equivalent nature of the phosphorus nuclei in the two triphenylphosphines. The IR and NMR spectroscopic data of the $[Ru(PPh_3)_2(L)(CO)]$ (L = L^1–L^4) complexes are therefore consistent with their composition and stereochemistry.

The $[Ru(PPh_3)_2(L)(CO)]$ (L = L^1–L^4) complexes are readily soluble in dichloromethane, acetone, chloroform, methanol, ethanol, acetonitrile, etc., producing bright-orange solutions. The electronic spectra of the complexes were recorded in dichloromethane solution. A representative spectrum is shown in Figure S1 in the Supporting Information, and the spectroscopic data are presented in Table 3. Each complex shows several intense absorptions in the visible and ultraviolet regions. To provide insight into the nature of these absorptions, TDDFT calculations were performed on all four $[Ru(PPh_3)_2(L)(CO)]$ (L = L^1–L^4) complexes by using the Gaussian 03 package,[7] with the phenyl rings of the triphenylphosphines being replaced by hydrogens to simplify the calculations. The results of the TDDFT calculations are summarized in Tables S3–S6 in the Supporting Information. The compositions of a few frontier orbitals of the $[Ru(PPh_3)_2(L)(CO)]$ (L = L^1–L^4) complexes are given in Table 4, and the contour plots of some selected molecular orbitals of $[Ru(PPh_3)_2(L^1)(CO)]$ are shown in Figure 7 with those of the remaining three complexes presented in Figures S2–S4 in the Supporting Information. The results obtained were found to be qualitatively similar for all four complexes, and hence only the case of $[Ru(PPh_3)_2(L^1)(CO)]$ is discussed here. The lowest-energy absorption at 554 nm is attributable to a combination of HOMO→LUMO and HOMO–1→LUMO transitions, and, based on the nature of the participating orbitals (Table 4 and Figure 7), the electronic excitation can be as-

Table 3. Electronic spectral and cyclic voltammetric data.

Complex	λ_{max} [nm] (ε [M^{-1} cm^{-1}])[a]	E [V][b]
$[Ru(PPh_3)_2(L^1)(CO)]$	554[c] (3050), 467 (6350), 341[c] (6540), 275[c] (19380), 236 (36650)	1.14,[d] 0.50[e] (70),[f] –1.71[g]
$[Ru(PPh_3)_2(L^2)(CO)]$	502[c] (4270), 461 (7650), 338[c] (6650), 276[c] (20290), 238 (36490)	1.35,[d] 0.68,[d] –1.74[g]
$[Ru(PPh_3)_2(L^3)(CO)]$	507[c] (3370), 470 (5300), 339[c] (4600), 274[c] (15330), 231 (36800)	1.17,[d] 0.72,[d] –1.75[g]
$[Ru(PPh_3)_2(L^4)(CO)]$	538[c] (3650), 482 (5090), 354[c] (5530), 287[c] (19170), 234 (33 260)	1.33,[d] 0.66,[d] –1.76[g]

[a] In dichloromethane. [b] Solvent: acetonitrile; supporting electrolyte: TBHP; reference electrode: SCE; scan rate: 50 mV s^{-1}. [c] Shoulder. [d] Anodic peak potential (E_{pa}) value. [e] $E_{1/2}$ = 0.5(E_{pa} + E_{pc}), in which E_{pc} is the cathodic peak potential. [f] ΔE_p value, for which ΔE_p = E_{pa} – E_{pc}. [g] E_{pc} value.

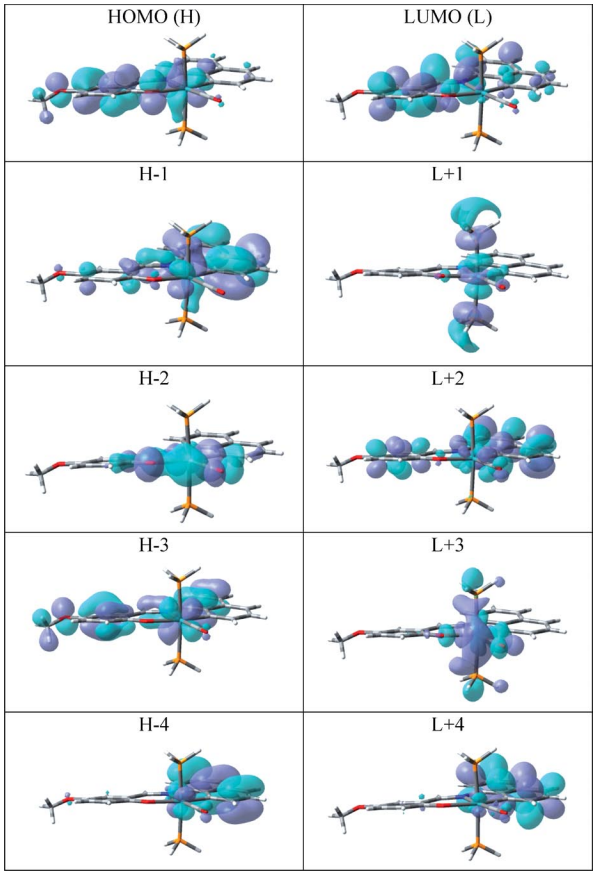

Figure 7. Contour plots of selected molecular orbitals of $[Ru(PH_3)_2(\mathbf{L^1})(CO)]$.

signed to a mixture of ILCT and MLCT transitions that primarily involve the ONC-coordinated aldimine ligand with a much lower contribution from the carbonyl and phosphine ligands. The next absorption at 467 nm is also of a similar nature. The absorption bands at 341 and 275 nm are primarily due to an admixture of ILCT and MLCT transitions, and the absorption at 236 nm can be ascribed to a mixture of LLCT, ILCT, and MLCT transitions.

Electrochemical Properties

The redox properties of the $[Ru(PPh_3)_2(\mathbf{L})(CO)]$ ($\mathbf{L} = \mathbf{L^1}$–$\mathbf{L^4}$) complexes were examined in acetonitrile solution (0.1 M TBHP) by cyclic voltammetry. The voltammograms of a selected complex are shown in Figure S5 in the Supporting Information and the voltammetric data are presented in Table 3. Each $[Ru(PPh_3)_2(\mathbf{L})(CO)]$ complex shows two oxidative waves and a single reduction wave. Based on the computed nature of the HOMO in these complexes (Table 4), the $0/1^+$ redox wave has been assigned to an oxidation of the coordinated aldimine ligand. Similarly, electron addition to the LUMO, which is delocalized mostly over the aldimine ligand (Table 4), leads to the reduction of the ancillary aldimine ligand. The $1^+/2^+$ oxidative response has tentatively been assigned to the second oxidation of the same coordinated aldimine ligand. In the $[Ru(PPh_3)_2(\mathbf{L^1})(CO)]$ complex, the first oxidation is quasi-reversible, based on an analysis of the current ratio as a function of scan rate. The other redox responses are irreversible. In the $[Ru(PPh_3)_2(\mathbf{L})(CO)]$ ($\mathbf{L} = \mathbf{L^1}$–$\mathbf{L^3}$) complexes, no systematic variation in the redox potential with the electron-withdrawing nature of the substituent R is observed, which is consistent with the HOMOs and LUMOs, which show no significant contributions from the R group.

Catalytic Transfer Hydrogenation

The transfer hydrogenation of aldehydes and ketones, with 2-propanol as solvent and reducing agent, has recently attracted considerable attention,[8] mostly due to the rela-

Table 4. Compositions of selected molecular orbitals of the complexes.

Complex	Fragments	Contribution [%] of fragments to							
		HOMO (H)	H–1	H–2	H–3	LUMO (L)	L+1	L+2	L+3
$[Ru(PH_3)_2(\mathbf{L^1})(CO)]$	Ru	20.6	20.1	33.5	16.5	4.7	25.8	14.2	22.2
	PH_3	5.7	7.3	0	0	2.0	56.3	1.0	41.0
	$\mathbf{L^1}$	72.5	72.6	44.3	82.5	90.8	10.9	67.8	12.8
	CO	1.2	0	22.2	1.0	2.5	7.0	17.0	24.0
$[Ru(PH_3)_2(\mathbf{L^2})(CO)]$	Ru	19.5	23.5	30.0	9.8	5.3	25.4	14.2	14.6
	PH_3	8.0	0	0	0	0	56.8	2.4	0
	$\mathbf{L^2}$	69.3	76.5	46.1	90.2	88.1	9.2	66.6	68.6
	CO	3.2	0	23.9	0	6.6	8.6	16.8	16.8
$[Ru(PH_3)_2(\mathbf{L^3})(CO)]$	Ru	20.2	22.2	30.4	19.0	0.7	25.5	13.9	33.7
	PH_3	8.1	0	0	0.6	0	58.1	0.4	14.3
	$\mathbf{L^3}$	70.6	77.8	46.1	78.3	94.6	9.0	69.8	12.9
	CO	1.1	0	23.5	2.1	4.7	7.4	15.9	39.1
$[Ru(PH_3)_2(\mathbf{L^4})(CO)]$	Ru	14.8	20.4	27.0	5.8	6.1	5.6	26.9	14.5
	PH_3	10.4	0	0	0	0	0	60.6	5.2
	$\mathbf{L^4}$	71.2	79.6	49.3	93.9	91.5	94.4	9.1	60.3
	CO	3.6	0	23.7	0.3	2.4	0	3.4	20.0

tively benign and green nature of the reagents. Although several transition-metal catalysts have been utilized for these reactions, complexes of ruthenium(II) remain a favorite choice.[9] Ruthenium-catalyzed transfer hydrogenation reactions require the intermediacy of a ruthenium–hydrido species, and hence complexes with a pre-existing Ru–H bond, or with potential for the in situ formation of such a bond, are suitable candidates for hydrogenation catalysis. Given the propensity for the in situ generation of ruthenium–hydrido species in the present group of $[Ru(PPh_3)_2(\mathbf{L})(CO)]$ complexes (see below), we wished to explore their catalytic potential in the transfer hydrogenation of carbonyl compounds. We began our study by examining the transfer hydrogenation of benzophenone to benzhydrol using $[Ru(PPh_3)_2(\mathbf{L^2})(CO)]$ as the catalyst precursor. Table 5 provides information on the impact of various reaction parameters on the efficiency of this process. After extensive optimization we found that 0.1 mol-% catalyst, 0.1 mmol KOH, 2-propanol as solvent, a reaction temperature of 85 °C, and a reaction time of 6 h furnished an excellent yield (100%) of the targeted product (entry 1). Upon lowering the catalyst loading, the reaction was found to be incomplete even after 15 h (entry 2) and decreasing the reaction time was also found to have a deleterious effect (entry 3). As expected, the desired reaction did not proceed at all in the absence of the ruthenium catalyst (entry 4). The base also plays an essential role, with no reaction observed in its absence (entry 5). KOH was found to be the most effective base, and its substitution by NaOH or K_3PO_4 led to a significant drop in yield (entries 6 and 7). The choice of 2-propanol as solvent was also found to be crucial as its replacement by ethanol or poly(ethylene glycol) lowered the yield considerably (entries 8 and 9).

Table 5. Screening of experimental conditions for the catalytic hydrogenation transfer.[a]

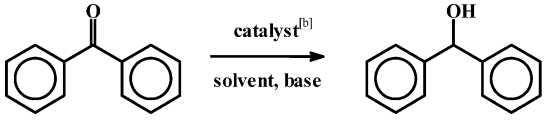

Entry	Catalyst [mol-%]	Solvent	Base	Time [h]	Yield[c] [%]
1	0.1	2-propanol	KOH	6	100
2	0.01	2-propanol	KOH	15	58
3	0.1	2-propanol	KOH	2	65
4	–	2-propanol	KOH	6	[d]
5	0.1	2-propanol	–	6	[d]
6	0.1	2-propanol	NaOH	6	71
7	0.1	2-propanol	K_3PO_4	6	27
8	0.1	ethanol	KOH	6	53
9	0.1	PEG	KOH	6	67

[a] Reaction conditions: benzophenone (1.0 mmol), base (0.1 mmol), solvent (5 mL), 85 °C. [b] Catalyst: $[Ru(PPh_3)_2(\mathbf{L^2})(CO)]$. [c] Determined by GC–MS. [d] No reaction observed.

The scope of these reactions is shown in Table 6. All four $[Ru(PPh_3)_2(\mathbf{L})(CO)]$ ($\mathbf{L} = \mathbf{L^1}$–$\mathbf{L^4}$) complexes display comparable catalytic efficiency, and only the results obtained with $[Ru(PPh_3)_2(\mathbf{L^2})(CO)]$ as catalyst are highlighted here.

Table 6. Catalytic transfer hydrogenation of aldehydes and ketones.[a]

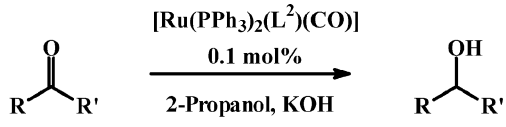

Entry	Substrate	Yield[b] (%)	TON[c]
1	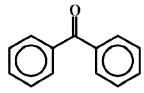	100	1000
2	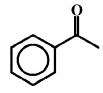	100	1000
3	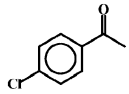	96	960
4	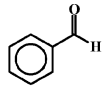	100	1000
5	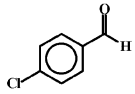	100	1000
6	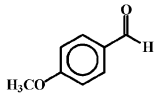	100	1000
7	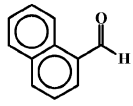	90	900
8	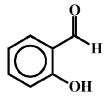	21	210
9	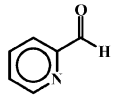	0	0
10	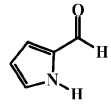	0	0
11		52	520
12		47	470
13	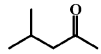	6	60

[a] Reaction conditions: aldehyde or ketone (1.0 mmol), KOH (0.1 mmol), 2-propanol (5 mL), 85 °C. [b] Determined by GC–MS. [c] TON = turnover number [(mol of product)/(mol of catalyst)].

Under the optimized conditions discussed above, benzophenone was hydrogenated to benzhydrol in excellent yield (entry 1). Acetophenone, *p*-chloroacetophenone, and *para*-substituted benzaldehydes (R = H, Cl, OCH_3) were also reduced with similar ease (entries 2–6). However, the reduction of 1-naphthaldehyde was slightly less facile (entry 7) and the reduction of salicylaldehyde turned out to be rather difficult (entry 8), whereas pyridine- and pyrrole-2-carbaldehyde did not undergo any reduction (entries 9 and 10). With cyclic aliphatic ketones, namely cyclohexanone and cyclohex-2-en-1-one, as substrates, the yield of the product alcohols decreased significantly (entries 11 and 12). With cyclohex-2-en-1-one, notably, only the ketone fragment underwent reduction, with the alkene fragment remaining unchanged. Methyl isobutyl ketone, an acyclic aliphatic ketone, was reduced, but in very poor yield (entry 13).

Although the mechanism of the observed catalysis is not yet completely clear to us, Scheme 2 shows the probable series of events using $[Ru(PPh_3)_2(\mathbf{L^2})(CO)]$ as the catalyst precursor. In the initial step, the $Ru–C_{naphthyl}$ bond in the native catalyst is believed to undergo protonolysis with 2-propanol to generate the intermediate **IM-1**, in which the isoproxide ligand is coordinated to the ruthenium through the oxygen atom. This species undergoes a β-hydride elimination of the coordinated isoproxide ligand, which is quite usual,[10] to afford the hydrido species **IM-2**. Insertion of the carbonyl substrate into the Ru–H bond takes place next to generate the corresponding aryloxo/alkoxo species **IM-3**. In the final step, elimination of the product alcohol takes place with simultaneous regeneration of the catalyst precursor.

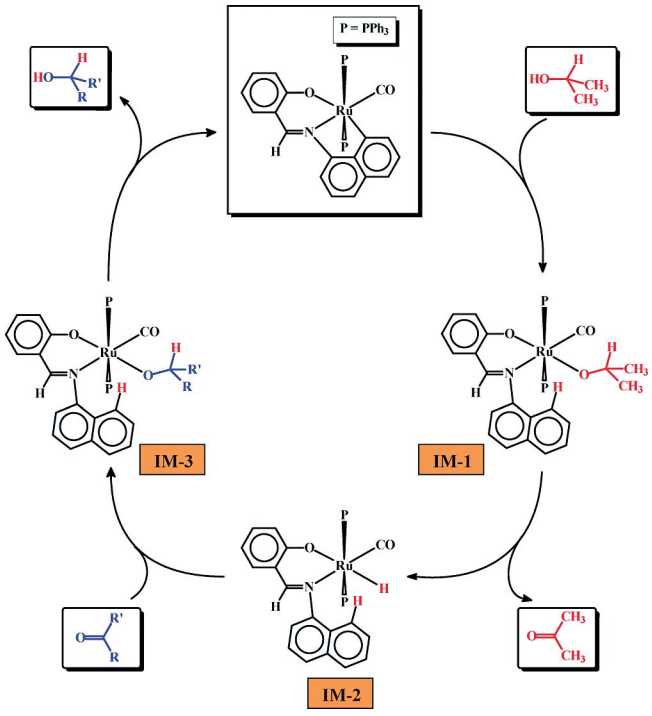

Scheme 2. Probable mechanism for the observed transfer hydrogenation reaction.

In the light of the proposed mechanism, the lower yield of the product alcohol with 1-naphthaldehyde as substrate (Table 6, entry 7) is likely to be due to the steric inhibition involved in the formation of the intermediate **IM-3**. The low yield observed for the reduction of salicylaldehyde (entry 8) and the absence of catalysis with pyridine- and pyrrole-2-carbaldehyde (entries 9 and 10) are probably due to catalyst deactivation through the coordination of these substrates, their potential to form chelates being well known. The difficulty encountered in the reduction of methyl isobutyl ketone (entry 13) can be attributed to its similarity with the competing byproduct, namely acetone, generated in the dehydrogenation of 2-propanol.

The present group of mixed-ligand cycloruthenated complexes, namely $[Ru(PPh_3)_2(\mathbf{L})(CO)]$ ($\mathbf{L} = \mathbf{L^1}–\mathbf{L^4}$), have thus been found to be efficient catalysts for the transfer hydrogenation of ketones and aldehydes using 2-propanol as the hydrogen donor. Variation of the substituents in the salicyl fragment (as in $H_2\mathbf{L^1}–H_2\mathbf{L^3}$), or substitution of the phenyl group (in $H_2\mathbf{L^2}$) by naphthyl (as in $H_2\mathbf{L^4}$), has not been found to have any observable influence on the catalytic efficiency of these complexes. The observed catalytic activity of these complexes is comparable to those of some recently reported ruthenium(II) complexes.[11] The noteworthy aspects of the observed catalysis are 1) good hydrogenation yields, 2) low catalyst loading, 3) relatively mild reaction conditions, and 4) a short reaction time.

Conclusions

This study has shown that, upon interaction with $[Ru(PPh_3)_2(CO)_2Cl_2]$, *N*-(naphthyl)salicylaldimine and related ligands $H_2\mathbf{L^1}–H_2\mathbf{L^4}$ readily undergo cycloruthenation by C–H bond activation at the *peri* position to afford complexes of the type $[Ru(PPh_3)_2(\mathbf{L})(CO)]$ ($\mathbf{L} = \mathbf{L^1}–\mathbf{L^4}$). This study has also revealed that the $Ru–C_{naphthyl}$ bond breaks in the presence of 2-propanol, and by virtue of this property the $[Ru(PPh_3)_2(\mathbf{L})(CO)]$ complexes can efficiently catalyze the transfer hydrogenation of ketones and aldehydes.

Experimental Section

Materials: Ruthenium trichloride was obtained from Arora Matthey, Kolkata, India. 1-Naphthylamine was purchased from Loba Chemie, Mumbai, India. Salicylaldehyde, 2-hydroxynaphthaldehyde, and triphenylphosphine were procured from Spectrochem, Mumbai, India. 5-Methoxysalicylaldehyde and 5-chlorosalicylaldehyde were procured from Alfa Aesar. The Schiff base ligands $H_2\mathbf{L^1}–H_2\mathbf{L^4}$ were prepared by reacting equimolar amounts of arylamine and aldehyde in hot ethanol. $[Ru(PPh_3)_2(CO)_2Cl_2]$ was prepared by following a reported procedure.[12] Tetrabutylammonium hexafluorophosphate (TBHP) procured from Aldrich and AR-grade acetonitrile procured from Merck (India) were used in electrochemical work. All other chemicals and solvents were reagent-grade commercial materials and used as received.

Physical Measurements: Microanalyses (C, H, and N) were performed by using a Heraeus Carlo Erba 1108 elemental analyzer. Magnetic susceptibilities were measured by using a Sherwood MK-1 balance. NMR spectra were recorded in $CDCl_3$ solution with a Bruker Avance DPX 300 NMR spectrometer. IR spectra were re-

corded with a Perkin–Elmer Spectrum Two IR spectrometer with samples prepared as KBr pellets. Electronic spectra were recorded with a JASCO V-570 spectrophotometer. Electrochemical measurements were conducted by using a CH Instruments model 600A electrochemical analyzer. A platinum disc working electrode, a platinum wire auxiliary electrode, and an aqueous saturated calomel reference electrode (SCE) were used in the cyclic voltammetry experiments. All electrochemical experiments were performed under nitrogen. All electrochemical data were collected at 298 K and are uncorrected for junction potentials. Geometry optimization by the density functional theory (DFT) method and electronic spectral analysis by TDDFT calculations were performed by using the Gaussian 03 (B3LYP/SDD-6-31G) package.[7] The different species in Scheme 1 were examined computationally by using the ONIOM method of Morokuma et al. using the Gaussian 03 software suite.[13] Here, all of the ruthenium-containing species were optimized by a two-level approach with the phenyl groups of the PPh_3 ligands treated as the lower of the two levels; all other compounds depicted in the scheme were optimized by ab initio DFT methods. For those species analyzed within the two-level treatment, we employed an ONIOM method that was defined by a B3LPY/PM6 composition. The phenyl groups (low level) were treated at the semi-empirical PM6 level of theory, whereas the remaining atoms (high level) were treated within the B3LYP framework. With respect to the high-level treatment of atoms, the ruthenium atoms were described by Stuttgart–Dresden effective core potentials (ecp) and a SDD basis set, whereas the 6-31+G(d′) basis set was employed for the remaining atoms. All of the species in Scheme 1 furnished fully optimized ground-state structures based on positive eigenvalues obtained from the analytical Hessian. The computed frequencies were used to make zero-point and thermal corrections to the electronic energies. GC–MS analyses were performed with a Perkin–Elmer CLARUS 680 instrument.

Preparations of Complexes: The $[Ru(PPh_3)_2(\mathbf{L})(CO)]$ ($\mathbf{L} = \mathbf{L^1}$–$\mathbf{L^4}$) complexes were prepared by following a general procedure. Specific details are given below for $[Ru(PPh_3)_2(\mathbf{L^1})(CO)]$.

$[Ru(PPh_3)_2(L^1)(CO)]$: Triethylamine (14 mg, 0.14 mmol) was added to a solution of $H_2\mathbf{L^1}$ (19 mg, 0.07 mmol) in hot 2-methoxyethanol (20 mL) followed by $[Ru(PPh_3)_2(CO)_2Cl_2]$ (50 mg, 0.07 mmol). The solution was then heated at reflux for 7 h to yield an orange solution. The solvent was removed under vacuum to afford a solid mass, which was subjected to purification by TLC on a silica plate. With hexane/benzene (1:1) as eluent, an orange band was separated, which was extracted with acetonitrile. Upon evaporation of the acetonitrile extract, $[Ru(PPh_3)_2(\mathbf{L^1})(CO)]$ was obtained as a crystalline orange solid.

$[Ru(PPh_3)_2(L^1)(CO)]$: Yield 27 mg, 43%. ^{1}H NMR:[14] δ = 3.57 (OCH_3), 5.61 (s, 1 H), 6.42 (d, J = 5.7 Hz, 1 H), 6.58 (dt, 2 H)*, 6.79 (t, J = 3.9 Hz, 1 H), 6.82 (d, J = 4.8 Hz, 1 H), 6.96 (d, J = 4.8 Hz, 1 H), 7.04–7.22 (2 PPh_3 + 1 H)*, 7.28 (s, azomethine), 7.38 (d, J = 4.8 Hz, 1 H) ppm. ^{13}C NMR: δ = 56.5, 108.3, 111.4, 116.0, 117.9, 119.0, 120.5, 123.6, 124.7, 125.8, 126.6, 127.4, 129.2, 132.7, 134.4, 138.6, 139.0, 147.0, 150.2, 156.3, 166.1, 168.0, 208.2 ppm. ^{31}P NMR: δ = 32.53 ppm. IR (KBr): $\tilde{\nu}$ = 1897, 1592, 1548, 1521, 1482, 1457, 1435, 1393, 1260, 1234, 1149, 1093, 813, 768, 741, 694, 611, 518, 498 cm^{-1}. $C_{55}H_{43}NO_3P_2Ru$ (928.1): calcd. C 71.12, H 4.63, N 1.51; found C 71.09, H 4.71, N 1.52.

$[Ru(PPh_3)_2(L^2)(CO)]$: Yield 23 mg, 39%. ^{1}H NMR: δ = 5.95 (t, J = 4.2 Hz, 1 H), 6.15 (d, J = 4.8 Hz, 1 H), 6.48 (d, J = 5.1 Hz, 1 H), 6.58 (t, J = 4.5 Hz, 1 H), 6.79 (d, J = 3.9 Hz, 1 H), 6.85 (dt, 2 H)*, 6.97 (d, J = 4.8 Hz, 1 H), 7.04–7.22 (2 PPh_3), 7.11 (t, J = 4.6 Hz, 1 H), 7.36 (s, azomethine), 7.39 (d, J = 4.8 Hz, 1 H) ppm. ^{13}C NMR: δ = 108.3, 111.6, 118.5, 120.8, 123.6, 124.6, 125.9, 126.6, 127.4, 128.4, 128.6, 129.2, 132.6, 133.6, 134.4, 135.9, 138.6, 139.1, 149.8, 157.1, 169.9, 207.6 ppm. ^{31}P NMR: δ = 32.64 ppm. IR (KBr): $\tilde{\nu}$ = 1900, 1603, 1550, 1521, 1482, 1435, 1396, 1233, 1146, 1093, 813, 768, 742, 694, 609, 519, 498 cm^{-1}. $C_{54}H_{41}NO_2P_2Ru$ (898.1): calcd. C 72.16, H 4.56, N 1.56; found C 72.09, H 4.59, N 1.57.

$[Ru(PPh_3)_2(L^3)(CO)]$: Yield 23 mg, 37%. ^{1}H NMR: δ = 6.10 (s, 1 H), 6.41 (d, J = 6.6 Hz, 1 H), 6.60 (t, J = 5.4 Hz, 1 H), 6.60 (t, J = 5.4 Hz, 1 H), 6.73 (d, J = 6.6 Hz, 1 H), 6.82 (dt, 2 H)*, 6.97 (d, J = 6.0 Hz, 1 H), 7.04–7.24 (2 PPh_3 + 1 H)*, 7.27 (s, azomethine), 7.41 (d, J = 6.0 Hz, 1 H) ppm. ^{13}C NMR: δ = 108.4, 115.3, 118.7, 121.1, 123.5, 125.8, 126.4, 126.6, 127.4, 128.5, 128.6, 129.3, 132.5, 133.4, 134.0, 134.2, 138.7, 138.9, 149.6, 155.9, 168.2, 207.8 ppm. ^{31}P NMR: δ = 33.98 ppm. IR (KBr): $\tilde{\nu}$ = 1900, 1602, 1549, 1509, 1482, 1435, 1395, 1230, 1156, 1094, 813, 767, 743, 695, 611, 518, 499 cm^{-1}. $C_{54}H_{40}ClNO_2P_2Ru$ (932.6): calcd. C 69.49, H 4.29, N 1.50; found C 69.51, H 4.21, N 1.48.

$[Ru(PPh_3)_2(L^4)(CO)]$: Yield 32 mg, 51%. ^{1}H NMR: δ = 6.63 (dt, 2 H)*, 6.77 (d + d, 2 H)*, 6.96–7.20 (2 PPh_3), 7.10 (t, J = 4.5 Hz, 1 H), 7.24 (d, J = 6.9 Hz, 1 H), 7.36 (d + d, 2 H)*, 7.46 (t + t, 2 H)*, 7.68 (d + d, 2 H)*; 8.35 (s, azomethine) ppm. ^{13}C NMR: δ = 108.3, 110.6, 118.8, 119.1, 120.7, 123.8, 125.0, 126.2, 126.4, 127.4, 127.9, 128.4, 128.6, 128.7, 129.3, 132.1, 132.2, 132.6, 134.4, 136.0, 138.4, 139.1, 150.4, 151.5, 171.1, 208.3 ppm. ^{31}P NMR: δ = 34.71 ppm. IR (KBr): $\tilde{\nu}$ = 1901, 1615, 1575, 1529, 1482, 1434, 1395, 1238, 1191, 1161, 1093, 827, 812, 767, 742, 694, 609, 518, 497 cm^{-1}. $C_{58}H_{43}NO_2P_2Ru$ (948.1): calcd. C 73.42, H 4.53, N 1.48; found C 73.51, H 4.50, N 1.52.

X-ray Crystallography: Single crystals of $[Ru(PPh_3)_2(\mathbf{L^1})(CO)]$, $[Ru(PPh_3)_2(\mathbf{L^2})(CO)]$, and $[Ru(PPh_3)_2(\mathbf{L^4})(CO)]$ were obtained by slow evaporation of solvents from solutions of the respective complexes in dichloromethane/acetonitrile (1:3). Selected crystal data and data collection parameters for $[Ru(PPh_3)_2(\mathbf{L^1})(CO)]$ are given in Table 7, and those for $[Ru(PPh_3)_2(\mathbf{L^2})(CO)]$ and $[Ru(PPh_3)$

Table 7. Crystallographic data for $[Ru(PPh_3)_2(\mathbf{L^1})(CO)]$.

Empirical formula	$C_{55}H_{43}NO_3P_2Ru$
M_r	928.91
Crystal system	triclinic
Space group	$P\bar{1}$
a [Å]	9.3791(4)
b [Å]	12.6129(6)
c [Å]	20.240(1)
α [°]	91.155(4)
β [°]	101.334(3)
γ [°]	107.804(3)
V [Å^3]	2226.9(2)
Z	2
$D_{calcd.}$ [mg m^{-3}]	1.385
$F(000)$	956
λ [Å]	0.71073
Crystal size [mm^3]	$0.21 \times 0.24 \times 0.25$
T [K]	296
μ [mm^{-1}]	0.470
Collected reflections	38857
R_{int}	0.107
Independent reflections	11030
$R1$[a]	0.0557
$wR2$[b]	0.1636
GOF[c]	0.95

[a] $R1 = \Sigma||F_o| - |F_c||/\Sigma|F_o|$. [b] $wR2 = [\Sigma\{w(F_o^2 - F_c^2)^2\}/\Sigma\{w(F_o^2)\}]^{1/2}$. [c] GOF = $[\Sigma\{w(F_o^2 - F_c^2)^2\}/(M - N)]^{1/2}$, in which M is the number of reflections and N is the number of parameters refined.

$_2$(**L^4**)(CO)] are shown in Table S7 in the Supporting Information. Data on all the crystals were collected with a Bruker SMART CCD diffractometer. X-ray data reduction, structure solution, and refinement were performed by using the SHELXS-97 and SHELXL-97 packages.[15] The structures were solved by direct methods. During refinement of the structure of [Ru(PPh$_3$)$_2$(**L^2**)(CO)], the lattice solvent molecules were found disordered and thus the SQUEEZE command of PLATON was applied before final solution of the structure.[16]

CCDC-989098 (for [Ru(PPh$_3$)$_2$(**L^1**)(CO)]), -989099 (for [Ru(PPh$_3$)$_2$(**L^2**)(CO)]), -989100 (for [Ru(PPh$_3$)$_2$(**L^4**)(CO)]) contain the supplementary crystallographic data for this paper. These data can be obtained free of charge from The Cambridge Crystallographic Data Centre via www.ccdc.cam.ac.uk/data_request/cif.

General Procedure for the Catalytic Transfer Hydrogenation Reactions: In a typical run, an oven-dried 10 mL round-bottomed flask was charged with the aldehyde/ketone (1 mmol), a known mol percent of the catalyst, and KOH (0.1 mmol) dissolved in 2-propanol (5 mL). The flask was placed in a preheated oil bath at the required temperature. After the specified time, the flask was removed from the oil bath and water (20 mL) was added, neutralized with 1 M HCl, and extracted with diethyl ether (4 × 10 mL). The combined organic layers were washed with water (3 × 10 mL), dried with anhydrous Na_2SO_4, and filtered. Diethyl ether was removed under vacuum and the residue obtained dissolved in hexane and analyzed by GC–MS.

Supporting Information (see footnote on the first page of this article): Selected bond lengths and bond angles for [Ru(PPh$_3$)$_2$(**L^2**)(CO)] and [Ru(PPh$_3$)$_2$(**L^4**)(CO)], some computed bond lengths and bond angles for the DFT-optimized structure of [Ru(PPh$_3$)$_2$(**L^3**)(CO)], results of TDDFT calculations, crystallographic data for [Ru(PPh$_3$)$_2$(**L^2**)(CO)] and [Ru(PPh$_3$)$_2$(**L^4**)(CO)], electronic spectrum of [Ru(PPh$_3$)$_2$(**L^1**)(CO)], contour plots of selected molecular orbitals of [Ru(PPh$_3$)$_2$(**L**)(CO)] (**L** = **L^2**–**L^4**), cyclic voltammograms of [Ru(PPh$_3$)$_2$(**L^2**)(CO)], and X-ray crystallographic data in CIF format.

Acknowledgments

The authors thank the reviewers for their constructive comments, which have been very helpful in preparing the revised manuscript. Financial assistance received from the Department of Science and Technology, Government of West Bengal, Kolkata [sanction number 746(Sanc.)/ST/P/S&T/2G-4/2013] is gratefully acknowledged. Financial support from the Robert A. Welch Foundation (grant number B-1093-MGR) and the National Science Foundation (NSF) (CHE-0741936) is acknowledged. J. D. thanks the Council of Scientific and Industrial Research (CSIR), New Delhi, for a fellowship [grant number 09/096(0702)/2011-EMR-I]. The authors thank Dr. Debajyoti Ghoshal and Dr. Pallab Mondal of Jadavpur University for their help with the crystal structure determination and TDDFT calculations, respectively.

[1] a) A. B. P. Lever, *Coord. Chem. Rev.* **2010**, *254*, 1397–1405; b) K. M. Lancaster, J. B. Gerken, A. C. Durrell, J. H. Palmer, H. B. Gray, *Coord. Chem. Rev.* **2010**, *254*, 1803–1811; c) S. L. F. Chan, Y. H. Kan, K. L. Yip, J. S. Huang, C. M. Che, *Coord. Chem. Rev.* **2011**, *255*, 899–919; d) G. C. Vougioukalakis, A. I. Philippopoulos, T. Stergiopoulos, P. Falaras, *Coord. Chem. Rev.* **2011**, *255*, 2602–2621; e) S. Takemoto, H. Matsuzaka, *Coord. Chem. Rev.* **2012**, *256*, 574–588; f) P. G. Bomben, K. C. D. Robson, B. D. Koivisto, C. P. Berlinguette, *Coord. Chem. Rev.* **2012**, *256*, 1438–1450; g) M. R. Gill, J. A. Thomas, *Chem. Soc. Rev.* **2012**, *41*, 3179–3192; h) Y. W. Zhong, C. J. Yao, H. J. Nie, *Coord. Chem. Rev.* **2013**, *257*, 1357–1372; i) B. J. Coe, *Coord. Chem. Rev.* **2013**, *257*, 1438–1458; j) J. A. Thomas, *Coord. Chem. Rev.* **2013**, *257*, 1555–1563.

[2] a) E. Colacino, J. Martinez, F. Lamaty, *Coord. Chem. Rev.* **2007**, *251*, 726–764; b) C. P. Lau, S. M. Ng, G. Jia, Z. Lin, *Coord. Chem. Rev.* **2007**, *251*, 2223–2237; c) D. Chatterjee, *Coord. Chem. Rev.* **2008**, *252*, 176–198; d) J. L. Boyer, J. Rochford, M. K. Tsai, J. T. Muckerman, E. Fujita, *Coord. Chem. Rev.* **2010**, *254*, 309–330; e) D. K. Dutta, B. Deb, *Coord. Chem. Rev.* **2011**, *255*, 1686–1712; f) C. Bruneau, M. Achard, *Coord. Chem. Rev.* **2012**, *256*, 525–536; g) F. B. Hamad, T. Sun, S. Xiao, F. Verpoort, *Coord. Chem. Rev.* **2013**, *257*, 2274–2292; h) P. Kumar, R. K. Gupta, D. S. Pandey, *Chem. Soc. Rev.* **2014**, *43*, 707–733.

[3] a) Y. Na, S. Park, S. B. Han, H. Han, S. Ko, S. Chan, *J. Am. Chem. Soc.* **2004**, *126*, 250–258; b) T. Hoshi, T. Nakazawa, I. Saitoh, Y. Mori, T. Suzuki, J. Sakai, H. Hagiwara, S. Akai, *Org. Lett.* **2008**, *10*, 2063–2066; c) M. Kawatsura, K. Kamesaki, M. Yamamoto, S. Hayase, T. Itoh, *Chem. Lett.* **2010**, *39*, 1050–1051; d) M. Kawatsura, M. Yamamoto, J. Namioka, K. Kajita, T. Hirakawa, T. Itoh, *Org. Lett.* **2011**, *13*, 1001–1003; e) J. Ito, K. Fujii, H. Nishiyama, *Chem. Eur. J.* **2013**, *19*, 601–605; f) S. Alvarez, S. Medina, G. Domínguez, J. P. Castells, *J. Org. Chem.* **2013**, *78*, 9995–10001; g) M. O. Simon, S. Darses, *J. Org. Chem.* **2013**, *78*, 9981–9985; h) S. Chanthamath, S. Takaki, K. Shibatomi, S. Iwasa, *Angew. Chem. Int. Ed.* **2013**, *52*, 5818–5821; *Angew. Chem.* **2013**, *125*, 5930; i) J. Zhang, S. Song, X. Wang, J. Jiaoa, M. Shi, *Chem. Commun.* **2013**, *49*, 9491–9493; j) C. Lubbe, A. Dumrath, H. Neumann, M. Schffer, R. Zimmermann, M. Beller, R. Kadyrov, *ChemCatChem* **2014**, *6*, 105–108; k) J. Jiang, X. Ma, C. Ji, Z. Guo, T. Shi, S. Liu, W. Hu, *Chem. Eur. J.* **2014**, *20*, 1505–1509; l) B. Chatterjee, C. Gunanathan, *Chem. Commun.* **2014**, *50*, 888–890.

[4] a) J. Costamagna, J. Vargas, R. Latorre, A. Alvarado, G. Mena, *Coord. Chem. Rev.* **1992**, *119*, 67–88; b) N. Hoshino, *Coord. Chem. Rev.* **1998**, *174*, 77–108.

[5] a) H. Brunner, M. Weber, M. Zabel, *Coord. Chem. Rev.* **2003**, *242*, 3–13; b) R. Drozdzak, B. Allaert, N. Ledoux, I. Dragutan, V. Dragutan, F. Verpoort, *Coord. Chem. Rev.* **2005**, *249*, 3055–3074.

[6] a) P. Gupta, S. Dutta, F. Basuli, S. M. Peng, G. H. Lee, S. Bhattacharya, *Inorg. Chem.* **2006**, *45*, 460–467; b) S. Nag, R. J. Butcher, S. Bhattacharya, *Eur. J. Inorg. Chem.* **2007**, 1251–1260.

[7] M. J. Frisch, G. W. Tracks, H. B. Schlegel, G. E. Scuseria, M. A. Robb, J. R. Cheeseman Jr., J. A. Montgomery, T. Vreven, K. N. Kudin, J. C. Burant, J. M. Millam, S. S. Iyengar, J. Tomasi, V. Barone, B. Mennucci, M. Cossi, G. Scalamani, N. Rega, G. A. Petersson, H. Nakatsuji, M. Hada, M. Ehara, K. Toyota, R. Fukuda, I. Hasegawa, M. Ishida, T. Nakajima, Y. Honda, O. Kitao, H. Nakai, M. Klene, X. Li, J. E. Knox, H. P. Hratchian, J. B. Cross, V. Bakken, C. Adamo, J. Jaramillo, R. Gomperts, R. E. Stratmann, O. Yazyev, A. J. Austin, R. Cammi, C. Pomelli, J. W. Ochterski, P. Y. Ayala, K. Morokuma, G. A. Voth, P. Salvador, J. J. Dannenberg, V. G. Zakrzewski, S. Dapprich, A. D. Daniels, M. C. Strain, O. Farkas, D. K. Malick, A. D. Rabuck, K. Raghavachari, J. B. Foresman, J. V. Ortiz, Q. Cui, A. G. baboul, S. Clifford, J. Cioslowski, B. B. Stefanov, G. Liu, A. Liashenko, P. Piskroz, I. Komaromi, R. L. Martin, D. J. Fox, T. Keith, M. A. Al-Laham, C. Y. Peng, A. Nanayakkara, M. Challacombe, P. M. W. Gill, B. Johnson, W. Chen, M. W. Wong, C. Gonzalez, J. A. Pople, *Gaussian 03*, revision D01, Gaussian, Inc., Pittsburgh, PA, **2003**.

[8] a) G. Erre, S. Enthaler, K. Junge, S. Gladiali, M. Beller, *Coord. Chem. Rev.* **2008**, *252*, 471–491; b) T. L. Church, P. G. Andersson, *Coord. Chem. Rev.* **2008**, *252*, 513–531; c) A. Fabrello, A. Bachelier, M. Urrutigoïty, P. Kalck, *Coord. Chem. Rev.* **2010**, *254*, 273–287; d) R. Malacea, R. Poli, E. Manoury, *Co-*

ord. Chem. Rev. **2010**, *254*, 729–752; e) S. Dayan, N. O. Kalaycioglu, J. Daran, A. Labande, R. Poli, *Eur. J. Inorg. Chem.* **2013**, 3224–3232; f) A. O. Ogweno, S. O. Ojwach, M. P. Akerman, *Dalton Trans.* **2014**, *43*, 1228–1237; g) M. Delgado-Rebollo, D. Canseco-Gonzalez, M. Hollering, H. Mueller-Bunz, M. Albrecht, *Dalton Trans.* **2014**, *43*, 4462–4473; h) M. M. Sheeba, M. M. Tamizh, L. J. Farrugia, A. Endo, R. Karvembu, *Organometallics* **2014**, *33*, 540–550; i) B. Ak, M. Aydemir, Y. S. Ocak, F. Durap, C. Kayan, A. Baysal, H. Temel, *Inorg. Chim. Acta* **2014**, *409*, 244–253.

[9] a) S. E. Clapham, A. Hadzovic, R. H. Morris, *Coord. Chem. Rev.* **2004**, *248*, 2201–2237; b) D. K. Dutta, B. Deb, *Coord. Chem. Rev.* **2011**, *255*, 1686–1712; c) A. Grabulosa, A. Mannua, E. Albericoc, S. Denurra, S. Gladiali, G. Muller, *J. Mol. Catal. A* **2012**, *363–364*, 49–57; d) M. E. Cucciolito, B. Panunzi, F. Ruffo, A. Tuzi, *Tetrahedron Lett.* **2013**, *54*, 1503–1506; e) A. Indra, P. Maity, S. Bhaduri, G. K. Lahiri, *ChemCatChem* **2013**, *5*, 322–330; f) C. Guyon, E. Métay, N. Duguet, M. Lemaire, *Eur. J. Org. Chem.* **2013**, 5439–5444; g) D. A. Cavarzan, F. D. Fagundes, O. Fuganti, C. W. P. da Silva, C. B. Pinheiro, D. F. Back, A. Barison, A. L. Bogado, M. P. de Araujo, *Polyhedron* **2013**, *62*, 75–82; h) S. O. Owalude, E. O. Odebunmi, U. B. Eke, A. L. Rheingold, N. Opembe, S. L. Suib, *J. Organomet. Chem.* **2013**, *739*, 21–25.

[10] a) J. J. Levison, S. D. Robinson, *J. Chem. Soc. A* **1970**, 2947–2954; b) R. Young, G. Wilkinson, *Inorg. Synth.* **1977**, *17*, 79–80; c) R. F. Winter, F. M. Hornung, *Inorg. Chem.* **1997**, *36*, 6197–6204; d) C. S. Yi, S. Y. Yun, I. A. Guzei, *Organometallics* **2004**, *23*, 5392–5395; e) T. Li, R. Churlaud, A. J. Lough, K. Abdur-Rashid, R. H. Morris, *Organometallics* **2004**, *23*, 6239–6247; f) R. CelenligilCetin, L. A. Watson, C. Guo, B. M. Foxman, O. V. Ozerov, *Organometallics* **2005**, *24*, 186–189.

[11] a) J. L. Pratihar, S. Bhaduri, P. Pattanayak, D. Patra, S. Chattopadhyay, *J. Organomet. Chem.* **2009**, *694*, 3401–3408; b) R. Manikandan, P. Viswanathamurthi, M. Muthukumar, *Spectroscopy* **2011**, *83*, 297–303; c) N. B. Jokić, M. Zhang-Presse, S. L. M. Goh, C. S. Straubinger, B. Bechlars, W. A. Herrmann, F. E. Kühn, *J. Organomet. Chem.* **2011**, *696*, 3900–3905; d) T. D. Nixon, M. K. Whittlesey, J. M. J. Williams, *Tetrahedron Lett.* **2011**, *52*, 6652–6654; e) E. Ö. Özcan, D. Mercan, N. Gürbüz, E. Çetinkaya, B. Çetinkaya, I. Özdemir, *Turkish J. Chem.* **2011**, *35*, 699–709; f) W. Du, L. Wang, P. Wu, Z. Yu, *Chem. Eur. J.* **2012**, *18*, 11550–11554; g) X. Guo, Y. Wang, D. Wang, L. Cai, Z. Chen, X. Hou, *Dalton Trans.* **2012**, *41*, 14557–14567; h) O. Dayana, S. Dayan, İ. Kanic, B. Çetinkaya, *Appl. Organomet. Chem.* **2012**, *26*, 663–670; i) R. N. Prabhu, R. Ramesh, *J. Organomet. Chem.* **2012**, *718*, 43–51; j) B. T. Kırkar, H. Turkmen, I. Kani, B. Cetinkaya, *Tetrahedron* **2012**, *68*, 8655–8662; k) J. DePasquale, N. J. White, E. J. Ennis, M. Zeller, J. P. Foley, E. T. Papish, *Polyhedron* **2013**, *58*, 162–170.

[12] N. Ahmad, S. D. Robinson, M. F. Uttley, *J. Chem. Soc., Dalton Trans.* **1972**, 843–847.

[13] M. Svensson, S. Humbel, R. D. J. Froese, T. Matsubara, S. Sieber, K. Morokuma, *J. Phys. Chem.* **1996**, *100*, 19357–19363.

[14] Chemical shifts are given in ppm and the multiplicity of the signals along with the associated coupling constants are given in parentheses. Overlapping signals are marked with an asterisk (*).

[15] a) G. M. Sheldrick, *SHELXS-97*, *Fortran programs for crystal structure solution and refinement*, University of Göttingen, Germany, **1997**; b) G. M. Sheldrick, *SHELXL-97*, *Fortran programs for crystal structure solution and refinement*, University of Göttingen, Germany, **1997**.

[16] A. L. Spek, *Acta Crystallogr., Sect. D* **2009**, *65*, 148–155.

Received: March 29, 2014
Published Online: ■

EurJIC European Journal of Inorganic Chemistry

Cycloruthenated Complexes

Keywords: Homogeneous catalysis / C–H activation / Hydrogenation / Ruthenium

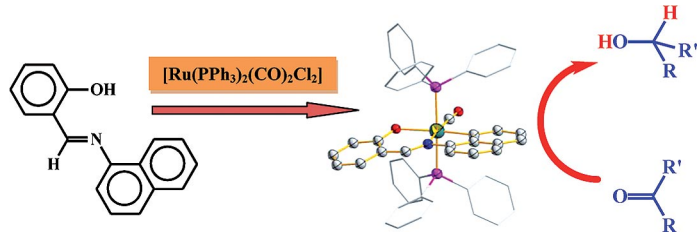

N-(Naphthyl)-4-R-salicylaldimines (R = OCH_3, H, Cl; $H_2\mathbf{L}^1$–$H_2\mathbf{L}^3$) and 2-hydroxy-*N*-(naphthyl)naphthaldimine ($H_2\mathbf{L}^4$) react with $[Ru(PPh_3)_2(CO)_2Cl_2]$, undergoing C–H bond activation at the *peri* position, to afford complexes of the type $[Ru(PPh_3)_2(\mathbf{L})(CO)]$ ($\mathbf{L} = \mathbf{L}^1$–$\mathbf{L}^4$), which can efficiently catalyze the transfer hydrogenation of carbonyl compounds.

